Dynamical Modeling and State Estimations of Gasoline and Ethanol Impingement Sprays in GDI Systems Using Experimental and State-Space Based Approaches*

Olena Kuzmych, Raouf Mobasheri, Abdel Aitouche,
Xiang Li, Dmytro Sobchuk, Lubov Dobrovolska and Lesya Fedik

***Abstract*— This study presents a comparative experimental and modeling analysis of the impingement spray characteristics of gasoline and ethanol using a high-pressure gasoline direct injection (GDI) injector. We develop Lyapunov-based approach to estimate key spray characteristics including rebound height with aid of MATLAB-based experimental data processing algorithms, both qualitative and quantitative assessments are provided, as well as a forecast of the state of these characteristics in future time intervals. We present a combined experimental and modeling approach for analyze the impingement spray behavior of gasoline and ethanol using a GDI injector taking into account base experimental results obtained in [3] where macroscopic properties were investigated via high-speed Schlieren imaging and Phase Doppler Particle Analysis (PDPA) across injection pressures ranging from 10 to 50 MPa. Data-driven modeling was supported by MATLAB-based polynomial curve fitting and system identification techniques. Key findings reveal that gasoline exhibits superior spray penetration and atomization compared to ethanol, particularly at ultra-high pressures. This suggests that gasoline atomization could significantly enhance combustion efficiency and emissions reduction in GDI engines.**

I. INTRODUCTION

The escalating global demand for sustainable energy sources has intensified research into renewable alternatives to fossil fuels. Bioethanol emerges as a promising candidate, capable of being blended with conventional gasoline to reduce petroleum dependency, minimize greenhouse gas emissions, and improve energy security. Its favorable combustion properties, high oxygen content, and renewability have led to increasing integration into automotive engines, particularly in Gasoline Direct Injection (GDI) systems [1]. Understanding the spray characteristics of alternative fuels such as ethanol under varying injection pressures is crucial to optimizing combustion, enhancing thermal efficiency, and minimizing emissions. Fuel spray behavior significantly affects the air–fuel mixture formation, influencing ignition, combustion quality, and pollutant formation. Our earlier investigations have shown that ethanol spray differs from gasoline in terms of atomization and droplet behavior, particularly under high injection pressures. For example, we demonstrated that ethanol yields finer droplets and more symmetric spray structures than gasoline at pressures up to 60 MPa, leading to better vaporization and potentially lower soot formation [2,3]. Further work has focused on both macroscopic and microscopic characteristics of ethanol and gasoline sprays in impingement configurations, showing that ethanol generally exhibits narrower cone angles and reduced wall wetting [4]. In another study, we employed high-speed Schlieren imaging and Phase Doppler Particle Analysis (PDPA) to analyze ethanol and gasoline sprays at up to 50 MPa, uncovering ubstantial differences in Sauter Mean Diameter (SMD), droplet velocity, and axial penetration [5]. We also explored the impact of flash boiling injection on butanol and ethanol spray dynamics, highlighting improvements in spray collapse and fuel–air mixing [6,7].

Therefore, in this paper, we continue our previous research concerning the comparison of different types of fuels, building upon our earlier work on the comparative investigation of the macroscopic and microscopic characteristics of impingement spray of gasoline and ethanol from a Gasoline Direct Injection (GDI) injector under injection pressure up to 50 MPa [3,4]. In parallel to experimental work, our group has contributed to the modeling of these complex spray and combustion phenomena. One focus has been the application of switched dynamical system theory to combustion modeling suitable for modeling processes such as mode transitions between fuels, injection timing, and ignition control [8]. State estimations are based on Lyapunov-based approach, it have been employed to ensure sate estimations, stability and robustness [9–15], this framework is relevant in automotive combustion applications.

In this work, we present a combined experimental and theoretical investigation of ethanol and gasoline spray dynamics in a GDI system operating under injection pressures up to 50 MPa. A switched linear system model is proposed, and a multiple Lyapunov function approach is used to estimate the system response at a final time from the initial condition. The model predictions are validated against Schlieren and PDPA experimental data. The results not only confirm the consistency of the modeling approach but also provide insights into control strategies for stable and efficient combustion with alternative fuels. This study builds upon and synthesizes our earlier work in spray diagnostics and hybrid system modeling, contributing to the development of cleaner and more efficient GDI combustion technologies.

*Research supported by ABC Foundation.

O. Kuzmych was with Lutsk National Technical University, Lutsk, Ukraine (corresponding author to provide e-mail: kuzmych79@gmail.com).

R. Mobasheri is with the ICL, Junia, Université Catholique de Lille, LITL, F-59000 Lille, France. (e-mails: raouf.mobasheri@junia.com)

Xiang Li is with Department of Mechanical Engineering, Nantong University, China. (e-mails: xiang.li@ntu.edu.cn)

A. Aitouche is with Automatic CRISTAL/JUNIA VILLENEUVE D'ASCQ, FRANCE 59650 (abdelouahab.aitouche@univ-lille.fr abdel.aitouche@junia.com).

D. Sobchuk and L. Dobrovolska are with Department of Electrical Engineering of Lutsk National Technical University Lutsk, Ukraine, (e-mail: dmytro.sobchuk.work@gmail.com, sobdim@gmail.com).

L. Fedik is with Automation and Computer-Integrated Technologies Department of Lutsk National Technical University Lutsk, Ukraine (e-mail: fedikltsia@gmail.com).

II. Experimental Setup and Method

A. Macroscopic Spray Analysis

A five-hole Gasoline Direct Injection (GDI) injector from a dual-injection spark-ignition (SI) engine was utilized in this study. The test fuels included commercial-grade gasoline and absolute ethanol.

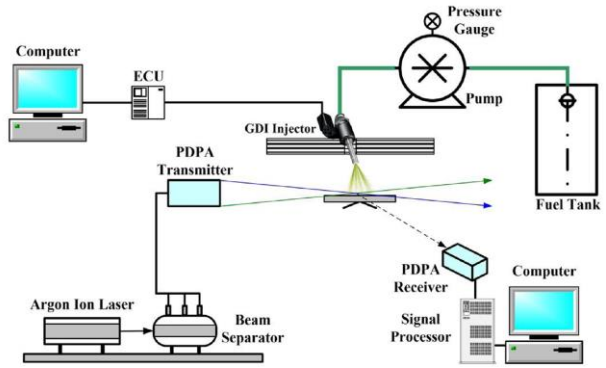

Figure 1. Experimental setup of macroscopic spray

Injection pressures of 10 MPa, 30 MPa, and 50 MPa were examined. Spray development was visualized using a high-speed Schlieren imaging system operating at 10,000 frames per second with a resolution of 768 × 768 pixels. The spray was directed toward a flat aluminum impingement plate positioned 33 mm downstream of the injector tip. The five spray jets were labeled Jet 1 through Jet 5. Jet 1 impinged on the wall at an inclined angle, while Jets 2–5 impacted perpendicularly. Key spray characteristics—including rebound height (HN, HF), lateral diffusion distance (DN, DF), spray area (AS), and pressure-time dynamics—were quantified through MATLAB-based image processing algorithms. Each experimental condition was repeated 30 times to ensure statistical reliability. Ambient conditions were controlled at 293 ± 0.5 K and atmospheric pressure (0.1 MPa). An air extraction system was employed to maintain safety and prevent accumulation of fuel vapors during testing.

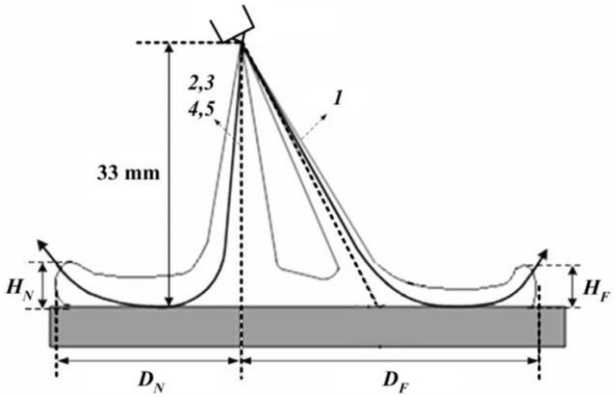

Figure 2. Determination of parameters of macroscopic spray

To investigate the macroscopic characteristics of gasoline and ethanol impingement sprays, a comprehensive experimental setup incorporating a Phase Doppler Particle Analyzer (PDPA) system was employed, as illustrated in Fig. 2. Each operating condition was repeated 30 times to ensure statistical robustness. The injector was mounted in a configuration mimicking a side-mounted orientation typically found in internal combustion engines. In this setup, Jets 2 through 5 impinged perpendicularly on the wall surface, whereas Jet 1 impacted at an oblique angle. The impingement surface was positioned 33 mm from the injector tip. The macroscopic evolution of the spray was evaluated using key parameters, including: **H_N, H_F:** near- and far-side rebound heights; **D_N, D_F:** lateral diffusion distances; AS: spray impingement area. These metrics enabled a detailed analysis of spray behavior under various fuel types and injection conditions, forming the basis for comparative evaluation and model validation.

B. Microscopic Spray Analysis

A PDPA system with a 1.3 W argon-ion laser and 180 MHz processor was used to analyze droplet sizes and velocities.

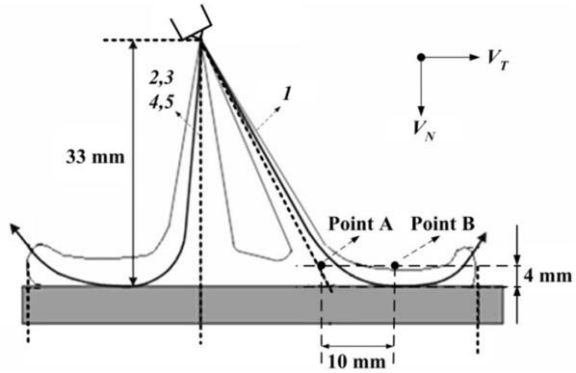

Figure 3. Determination of parameters of microscopic spray

Measurement points A and B were placed 4 mm above the wall. Key parameters included droplet diameter (Dd), Sauter mean diameter (DSMD), normal and tangential velocities (VN, VT), and their probability distributions.

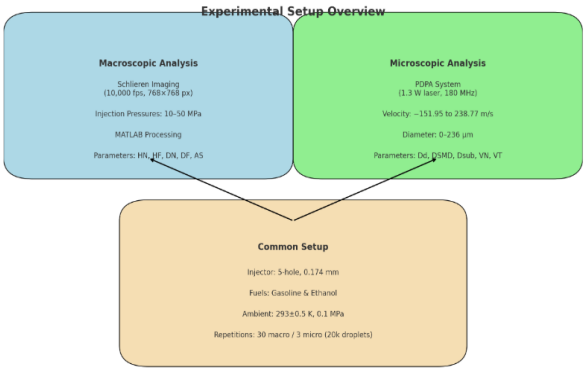

Figure 4. Experimental setup overview.

At least 20,000 valid droplet measurements were collected per condition, with three repeated trials for each setup. More information could be found in the paper [3]. The Fig. 4 represents the overview of macroscopic and microscopic spray.

III. Research Methodology

In this section we use tools of quadratic multiple Lyapunov functions for obtain estimation of solution. Therefore we analyze a switched system composed of

several linear subsystems, each active over finite time intervals., $T_i = [t_{i-1}, t_i]$, $i = \overline{1,N}$. The moments of time $t_1, t_2, ..., t_i, ..., t_N$ are called *switching moments*. Such switched system can be written as a family of systems which are described by

$$\dot{x}(t) = A_i x(t), \ i = \overline{1,N}, \ t \geq 0 \qquad (1)$$

where $x(t) \in R^n$, A_i - constant matrices. For solutions $x = x(x_0, t)$ the continuity condition

$$\lim_{s \to +0} x(t_i - s) = \lim_{s \to +0} x(t_i + s), i = \overline{1,N} \qquad (2)$$

holds at switching moments. It is known that for the linear system with constant coefficients

$$\dot{x}(t) = Ax(t), x(t) \in R^n, t \geq 0$$

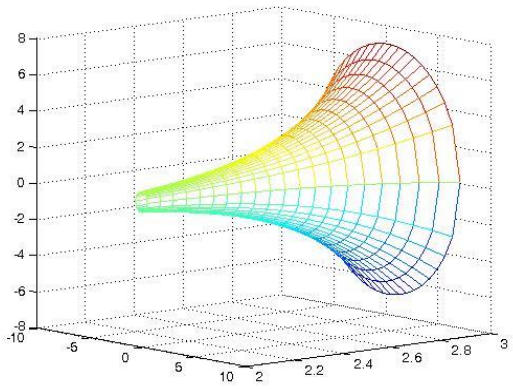

Figure 5. View of Lyapunov Function

A general solution is $x(x_0, t) = e^{At} x_0$ where matrix exponential has the form

$$e^{At} = I + A\frac{t}{1!} + A^2\frac{t^2}{2!} + \cdots + A^k\frac{t^k}{k!} + \cdots$$

And the solution of the system can be estimated with the use of the Lyapunov function, which has a quadratic form

$$V(x,t) = x_0^T x_0 = \left(e^{-At}x\right)^T \left(e^{-At}x\right),$$

or $V(x,t) = x^T H(t) x, \ H(t) = e^{-A^T t} e^{-At}$. This Lyapunov function describes the evolution the most exactly. The space $V(x,t) < \alpha$ is a middle of ellipse which goes out from the neighbourhood $|x_0| < \alpha$ but changes along the solutions $x = x(x_0, t)$. The multiple Lyapunov functions of the switched system are shown on Fig. 5.

Theorem 1. Let the initial state of the switched system (1) satisfy the condition $|x(0)| < \delta$. Then at $t = t_N$ inequality

$$|x(t_N - 0)| < \frac{\delta}{\sqrt{\prod_{i=1}^{N} \lambda_{\min}[H_i(t_i)]}}, \qquad (4)$$

holds, where $H_i(t_i) = e^{-A_i^T (t_i - t_{i-1})} e^{-A_i (t_i - t_{i-1})}, \ i = \overline{1,N}, t_0 = 0$.

Proof. For the first time interval of evolution we have:

$$\dot{x}(t) = A_1 x(t), \ x(t) \in R^n, \ t_0 \leq t < t_1, \ t_0 = 0. \qquad (5)$$

We select the Lyapunov function as

$$V(x,t) = x^T H_1(t) x, \ H_1(t) = e^{-A_1^T t} e^{-A_1 t}$$

under the condition

$$\lambda_{\min}[H_1(t)] |x(t)|^2 \leq V_1(x(t),t) \leq \lambda_{\max}[H_1(t)] |x(t)|^2.$$

The derivative of $V_1(x,t)$ for the subsystem (5) yields

$$\frac{d}{dt} V_1(x(t),t) = \dot{x}^T(t) H_1(t) x(t) +$$

$$+ x^T(t) \frac{d}{dt} H_1(t) x(t) + x^T(t) H_1(t) \dot{x}(t) \equiv 0$$

Therefore, at arbitrary $t: \ 0 \leq t < t_1$ Lyapunov function:

$$V_1(x(t),t) \equiv V_1(x(0),0) = \text{const}, \ 0 \leq t < t_1.$$

We get

$$\lambda_{\min}\left[H_1(t_1 - 0)\right] \left|x(t_1 - 0)\right|^2 \leq V_1(x(t_1 - 0), t_1 - 0) =$$

$$= V_1(x(0),0) \leq \lambda_{\max}\left[H_1(0)\right] \left|x(0)\right|^2 = \left|x(0)\right|^2$$

And for the first time interval we get inequality

$$|x_1(t_1 - 0)| \leq \frac{|x(0)|}{\sqrt{\lambda_{\min}[H_1(t_1)]}}.$$

We consider the second time interval, and the subsystem

$$\dot{x}(t) = A_2 x(t), \ x(t) \in R^n, \ t_1 \leq t < t_2. \qquad (6)$$

The Lyapunov function has a form

$$V_2(x,t) = x^T H_2(t) x, \ H_2(t) = e^{-A_2^T (t - t_1)} e^{-A_2 (t - t_1)}.$$

The bilateral inequality

$$\lambda_{\min}[H_2(t)] |x(t)|^2 \leq V_2(x(t),t) \leq \lambda_{\max}[H_2(t)] |x(t)|^2.$$

The derivative of function $V_2(x,t)$ for subsystem (6) is

$$\frac{d}{dt} V_2(x(t),t) \equiv 0, \ t_1 \leq t < t_2,$$

And $V_2(x(t),t) \equiv V_2(x\ (t_1 + 0), t_1 + 0) = \text{const}, \ t_1 \leq t < t_2$.

We have

$$\lambda_{\min}[H_2(t_2 - 0)] |x(t_2 - 0)|^2 \leq V_2(x(t_2 - 0), t_2 - 0) =$$

$$= V_2(x(t_1 + 0), t_1 + 0) \leq$$

$$\leq \lambda_{\max}[H_2(t_1 + 0)] |x(t_1 + 0)|^2 = |x(t_1 + 0)|^2.$$

And for the second time interval we get

$$\left|x(t_2 - 0)\right| \leq \frac{\left|x(t_1 + 0)\right|}{\sqrt{\lambda_{\min}\left[H_2(t_2)\right]}}.$$

Using the continuity of the state at t_1 we relate the Lyapunov functions of successive intervals

$$|x_2(t_2 - 0)| \leq \frac{|x(0)|}{\sqrt{\lambda_{\min}[H_2(t_2)] \lambda_{\min}[H_1(t_1)]}}$$

holds at the switched moment. Continuing the process farther, we get the estimation:

$$|x_N(t_N - 0)| \leq \frac{|x(0)|}{\sqrt{\prod_{i=1}^{N} \lambda_{\min}[H_i(t_i)]}}, \qquad (7)$$

concluding the proof of Theorem 1.

The results of research into the monitoring of the state of the macroscopic characteristics of gasoline and ethanol

impingement sprays, make it possible to justify the requirements for functional characteristics of the system using mathematical modeling methods.

IV. Main Results

A. Polynomial modelingof the system

Using the available MatLab tools we calculate the values needed. For predicting the behavior of parameters, we make mathematical modeling using MatLab appropriate tools. On the following figures, the plotting of the datasets is presented. The data frame of daily time is [0-24] hours. We make fit in curve of the loaded data using the appropriate Curve Fitting Toolbox. We use polynomial for interpolation and characterize data using a global fit to obtain a simple empirical model. The main advantage of selected polynomial fit is reasonable flexibility for data that is not too complicated. Analyzing the datasets obtained in [3] we obtain resulting linear model which is a polynomial of the degree 3 in a following form

$$f(x) = p_1*x^3 + p_2*x^2 + p_3*x + p_4.$$

Experiment 1.

At this experiment for the 10-E data the coefficients are calculated with 95 percents of confidence bounds:
Coefficients: p_1*=0.31 (-0.7978, 1.435);* p_2*=-3.63 (-10.71, 3.432);* p_3*=7.23 (2.81, 31.64);* p_4*=-8.96 (-18.38, 0.4533)* .

The goodness of the fit are defined by SSE: 1.1527; RSQUARE: 0.9951; DFE: 14; ADJRSQUARE: 0.9940; RMSE: 0.2869.

Experiment 2.

At this experiment for the 10-G data the coefficients (with 95% confidence bounds) are: p_1 = 0.5326 (-0.3249, 1.39); p_2 = -5.562 (-10.99, -0.1322); p_3 = 22.42 (11.35, 33.5); p_4 =-12.73 (-19.96, -5.495).

The GOF is defined by SSE: 0.6800; RSQUARE: 0.9972; DFE: 14; ADJRSQUARE: 0.9966; RMSE: .2204

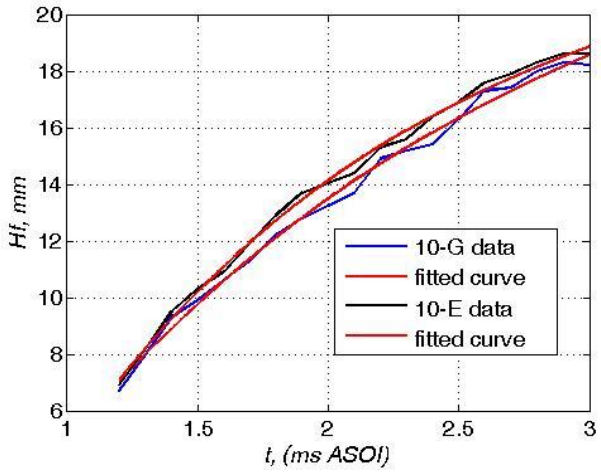

Figure 6. Evolution of data and fitted curve of experiments 1 and 2.

Experiment 3.

At this experiment for the 30-E data the coefficients are calculated with 95 percents of confidence bounds: p_1 = 1.413 (0.8477, 1.979); p_2 = -10.58 (-13.82, -7.35); p_3 = 31.49 (25.69, 37.29); p_4 = -12.4 (-15.62, -9.185).

GOF is defined by SSE: 1.5351; RSQUARE: 0.9975; DFE: 18; ADJRSQUARE: 0.9971; RMSE: 0.2920.

Experiment 4.

At this experiment for the 30-G data the coefficients are calculated with 95 percents of confidence bounds: p_1= 0.3592 (-0.3218, 1.04); p_2 = -4.643 (-8.538, -0.7468); p_3 = 21.18 (14.2, 28.17); p_4 = -6.502 (-10.38, -2.628).

GOF is defined by SSE: 2.2268; RSQUARE: 0.9964; DFE: 18; ADJRSQUARE: 0.9958; RMSE: 0.3517.

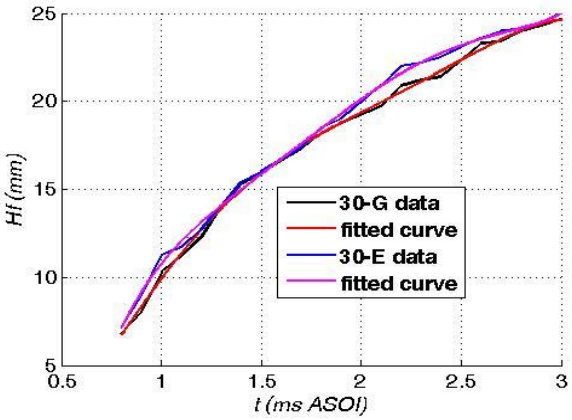

Figure 7. Evolution of data and fitted curve of experiments 3 and 4.

Experiment 5.

At this experiment for 50-E, 50-G data the coefficients are calculated with 95 percents of confidence bounds: p_1 = 2.111 (1.403, 2.82); p_2 =-14.56 (-18.51, -10.62); p_3 = 38.11 (31.28, 44.94); p_4 =-13.09 (-16.7, -9.485). GOF is defined by SSE: 3.4443; RSQUARE: 0.9953; DFE: 19; ADJRSQUARE: 0.9945; RMSE: 0.4258.

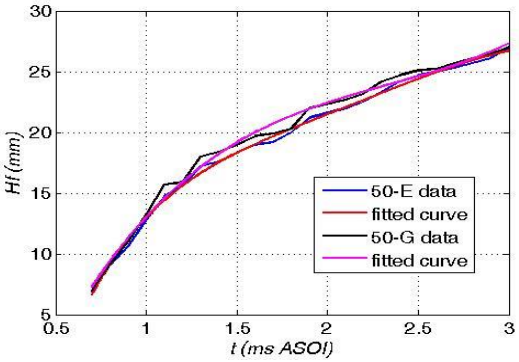

Figure 8. Evolution of data and fitted curve of experiment 5.

B. System Identification

We make the estimation data using System Identification Toolbox of MatLab by using state-space model, polynomial models, nonlinear models.

1) Nonlinear Model.

The data was estimated by using the MatLab Toolbox System Identification with Hammerstein-Wiener nonlinear model. Then we obtain a nonlinear model with nonlinearity as piecewise linear. We obtain the following model parameters:

- *Estimation data* with 23 samples.
- *Input nonlinearity*: piecewise linear with 10 units and unspecified break points.
- *Results*: Final prediction error (FPE): 77.74, Loss function: 15.03; Fit to working data: 80.67%.

The nonlinear model facilitates estimation of nonlinear black box models as Hammerstein-Wiener models. It operates on working data in the System Identification Toolbox to perform the estimation.

2) State space model.

Continuous terms were identified using linear state-space model:

$$\frac{dx}{dt} = Ax(t) + Bu(t) + Ke(t),$$

$$y(t) = Cx(t) + e(t), \; C = (4.22 \quad -0.92)$$

$$A = \begin{pmatrix} 0.07 & 0.17 \\ -0.10 & -1.21 \end{pmatrix}; \; B = \begin{pmatrix} 1.05 \\ -8.49 \end{pmatrix}, \; K = \begin{pmatrix} 0.15 \\ 0.25 \end{pmatrix}.$$

The plots show the simulated (predicted) outputs of obtained model. The models are fed with inputs from the validation data set, whose output is plotted in black. FPE estimates how well a model, trained on a finite data set, will predict future data. The precise definition of the fit is:

Fit = [1 – Norm(Y - Yhat)/Norm*(Y -mean(Y))]*100,*

where Y is the measured output Yhat is the simulated/predicted model output.

The Hammerstein-Wiener Nonlinear Model has the following accuracy and simulation parameters: *Fit: 80.67%, FPE: 77.74; and the state space model has: Fit: 90.02%, FPE: 0.8174*

3) Discrete-time ARX model.

Discrete-time ARX model that we obtain is the following:

$$A(z)y(t)=B(z)u(t)+e(t)$$

$$A(z)=1-1.119z^{-1}+3.017z^{-2}+1.831z^{-3}-4.874z^{-4}$$

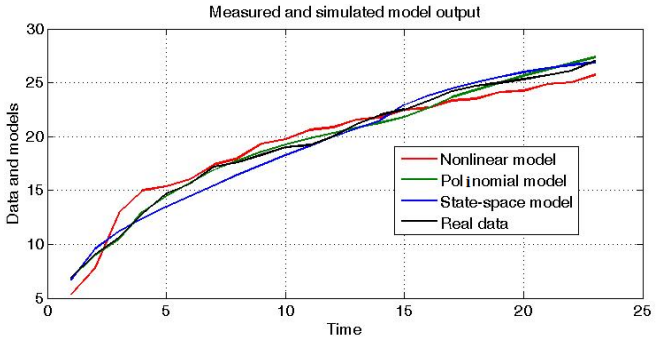

Figure 9. Comparison of various models

This model demonstrates best overall performance with used polynomial order *na*=4, *nb*=4, *nk*=1, Fit: 94.7%, FPE: 0.1503. The comparison results of these 3 methods and the real experimental data are presented on Fig. The fitting quality are: 92.62% for the Polynomial Models tool result; 87.29% for the state-space model; 80.67% for the obtained nonlinear model. For the dynamic simulation of SS-model we use MATLAB environment and solver *ode45*. Besides the Control System Toolbox was used to solve the appropriate Riccati equations. With aid of MATLAB function *care* the solution *X* of the relative Riccati equation was obtained.

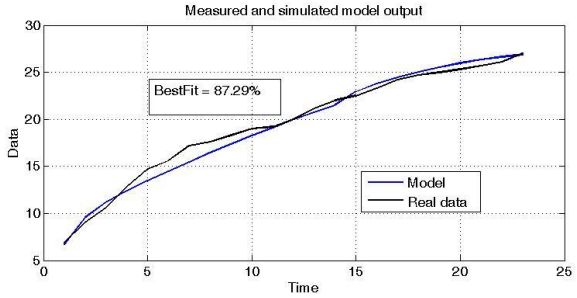

Figure 10. SS-model

Using *care*-algorithm the solution has been obtaibed by choosing the weighting matrices *R* and *Q* . The system state has to be evaluated by control inputs center and then it sets the control gain matrix parameters. The obtained simulation experimental results are presented in the following section.

V. Experimental validation

In this section we find the estimation of rebound height HF characteristic with aid of obtained dynamical system solution with a time-switch controller described by linear subsystem. Using the estimations for separate subsystems, which are obtained with the method of Lyapunov functions, and using the continuity condition of solution at the switching moments, we get the estimation of the origin switched system solution at the final moment depending on initial state. Using the Lyapunov function of quadratic form with matrix exponential the estimations of solution are obtained. For the known matrices

$$\mathrm{A} = \begin{bmatrix} 0.07 & 0.17 \\ -0.1 & -1.21 \end{bmatrix}, \; \mathrm{B} = \begin{bmatrix} 1.05 \\ -8.49 \end{bmatrix}$$

we choose the matrices: $\mathrm{Q} = \begin{bmatrix} 0.001 & 0 \\ 0 & 0.1 \end{bmatrix}, \; R = [20] \cdot$

And as a result we obtain the stabilized control gain K =[-1.4113, -0.2046], u_1= -38.8719, u_2= 314.3068. The simulation results are presented on Fig.11. Using the Rikkati equations we obtain the stabilized system:

$$\mathrm{A}_1 = \begin{bmatrix} 1.4146 & 0.3522 \\ -10.9721 & -2.6831 \end{bmatrix}$$

State estimations and prediction are the following:

$$V(x,t) = x^T H_1(t) x, \;\; H_1(t) = e^{-A_1^T t} e^{-A_1 t}$$

$$|x_1(t_1 - 0)| \le \frac{|x(0)|}{\sqrt{\lambda_{\min}[H_1(t_1)]}}$$

We calculate:

1. For the time interval $(t_1 - t_0) = 1$ we obtain $\lambda_{\min}[H_1(t)] = 0.49$. If the initial deviation is $|x(0)| = 26$; The calculated estimation is: $|x_1(t_1)| = \frac{26}{0.7} = 37.14 \cdot$ The appropriate Lyapunov function id presented on Fig.11.

2. At the initial deviation is $|x(0)| = 26$, for the time interval $(t_1 - t_0) = 1.5$ we calculate $\lambda_{\min}[H_1(t)] = 0.3$.

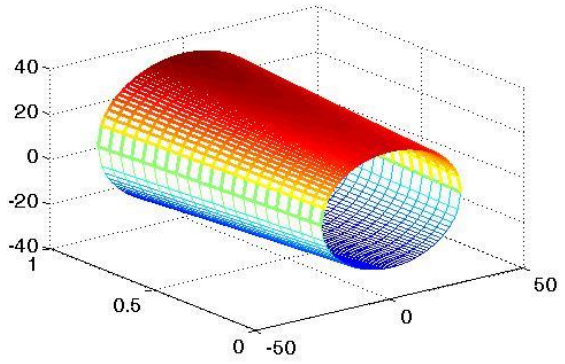

Figure 11. Lyapunov function for the $(t_1 - t_0) = 1$.

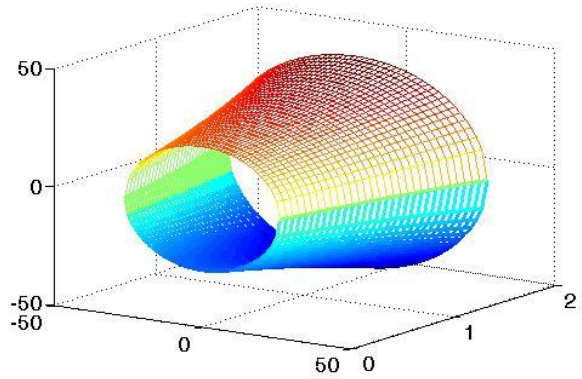

Fig.12. Lyapunov function for the $(t_1 - t_0) = 1.5$.

State estimations and prediction are the following: $|x_2(t_2)| = \frac{26}{0.54} = 48.14$. The appropriate Lyapunov function is presented on Fig.12. Obtaining the state estimations gives us key spray characteristics including rebound height HF, were quantified through MATLAB-based experimental data processing algorithms. At the same time, both qualitative and quantitative assessments are provided, as well as a forecast of the state of these characteristics in future time intervals.

VI. Conclusion

This study presented a combined experimental and modeling approach to analyze the impingement spray behavior of gasoline and ethanol using a GDI injector taking into account base experimental results obtained in [3]. A Lyapunov-based approach was developed to estimate key spray characteristics including rebound height with aid of MATLAB-based experimental data processing algorithms. At the same time, both qualitative and quantitative assessments are provided, as well as a forecast of the state of these characteristics in future time intervals. Experimental investigations, conducted through high-speed Schlieren imaging and Phase Doppler Particle Analysis (PDPA), demonstrated that gasoline sprays generally exhibited greater rebound heights and more effective atomization compared to ethanol, particularly at elevated injection pressures. The consistency between the experimental findings and model predictions validates the use of Lyapunov-based analysis in capturing key features of spray dynamics. These insights enhance our understanding of fuel–wall interaction and can inform future injector design, control strategies, and emission mitigation measures. As a direction for future research, the modeling framework will be extended to incorporate nonlinear dynamics or data-driven switching laws to further improve its predictive capabilities.

References

[1] H. Chen, C.Wang, X. Li, Y. Li, M. Zhang, , Z. Peng, Y. Pei, Z. Ma, X. Zhang, P. Ni. Quantitative Analysis of Water Injection Mass and Timing Effects on Oxy-Fuel Combustion Characteristics in a GDI Engine Fuelled with E10. Sustainability, 15(13), 2023. pp.10290.

[2] X. Li, X.Zhang, T. Zhang, C. Ji, P. Ni, W. Li, Y. Pei, Z. Peng, R. Mobasheri. Insights into Microscopic Characteristics of Gasoline and Ethanol Spray from a GDI Injector Under Injection Pressure up to 50 MPa. Sustainability, 16(21), 2024. p. 9471.

[3] X. Li, D. Li, P. Dimitriou, T. Ajmal, A. Aitouche, R. Mobasheri, O. Rybdylova, et al. Comparative Investigation on Macroscopic and Microscopic Characteristics of Impingement Spray of Gasoline and Ethanol from a GDI Injector Under Injection Pressure up to 50 MPa. Energy Reports, 9, 2023, pp.1910–1918.

[4] X. Li, D. Li, J. Liu, T. Ajmal, A. Aitouche, R. Mobasheri, O. Rybdylova, Y. Pei, Z. Peng. Comparative Study on the Macroscopic Characteristics of Gasoline and Ethanol Spray from a GDI Injector under Injection Pressures of 10 and 60 MPa. ACS Omega, no.7(10), 2022, pp. 8864–8873.

[5] X. Li, Z. Sun, S. Yang, H. Wang, & M. Nour. Flash Boiling Combustion of Isomeric Butanol and Gasoline Surrogate Blends Using Constant Volume Spray Chamber and GDI Optical Engine. Fuel, no.286, 2021, pp. 119328.

[6] X. Li, Z. Sun, M. Cui, S.Yang, D. Hung, M. Xu. Effect of Flash Boiling Injection on Combustion and PN Emissions of DISI Optical Engine Fueled with Butanol Isomers/TPRF Blends. Proceedings of the Combustion Institute, no. 38(4), 2021, pp.5923–5931.

[7] X. Li, Z. Sun, M. Cui, S. Yang, D. Hung, M. Xu. Combustion and Emissions of Isomeric Butanol/Gasoline Surrogate Blends on an Optical GDI Engine. Fuel, no. 272, 2021, p. 117635.

[8] D. Liberzon, A. S. Morse. Basic Problems in Stability and Design of Switched Systems. IEEE Control Systems Magazine, no. 19(5), 1999, pp. 59–70.

[9] R. A. DeCarlo, M. S. Branicky, S. Pettersson, B. Lennartson. Perspectives and Results on the Stability and Stabilizability of Hybrid Systems. Proceedings of the IEEE, no. 88(7), 2000. pp. 1069–1082.

[10] R. Goebel, R. G. Sanfelice, A. R. Teel. Hybrid Dynamical Systems. IEEE Control Systems Magazine, no. 29(2), 2009. pp. 28–93.

[11] R. Shorten, F. Wirth. A Survey on Switched and Hybrid Systems. Automatica, no. 41(4), 2005, pp. 575–582.

[12] H. Lin, P. J. Antsaklis. Stability and Stabilizability of Switched Linear Systems: A Survey of Recent Results. IEEE Trans. on Automatic Control, no. 54(2), 2009, pp. 308–322.

[13] O. Kuzmych, A. E. Hajjaji, A. Aitouche and J. Bosche, "Sum of squares based nonlinear control design. Application to biodiesel engine," 2015 4th International Conference on Systems and Control (ICSC), Sousse, Tunisia, 2015, pp. 50-57, doi: 10.1109/ICoSC.2015.7153278.

[14] O. Kuzmych, A. Aitouche and L. Cheng, "Robust nonlinear control design for turbocharged biodiesel engine," 3rd International Conference on Systems and Control, Algiers, Algeria, 2013, pp. 395-400, doi: 10.1109/ICoSC.2013.6750889.

[15] O. Kuzmych and A. Aitouche, "CLF-based nonlinear control design for turbocharged Diesel engine," 21st Mediterranean Conference on Control and Automation, Platanias, Greece, 2013, pp. 1484-1489, doi: 10.1109/MED.2013.6608917.